ARTICLE

Preparation of Manganese-doped ZnSe Precursor Nanoribbon Bundles and Investigation of its Magneto-optical Properties

Yuan-yuan Zhang, Jia-fu Chen*, Xu-sheng Zheng, Xue-hui Dong

Hefei National Laboratory for Physical Sciences at Microscale, University of Science and Technology of China, Hefei 230026, China

(Dated: Received on November 25, 2006; Accepted on January 22, 2007)

Mn^{2+}-doped ZnSe ethylenediamine-intercalated precursor nanoribbon bundles ($Mn_xZn_{1-x}Se{\cdot}en_3$, en=ethylenediamine) were prepared through an improved solvothermal route, which is time-saving and more efficient compared with the traditional route. XPS, TGA, and FESEM were used to characterize morphology and composites of the precursor and it was proved that the doping process was successful. Electron paramagnetic resonance and photoluminescence (PL) spectra were used in a detailed experiment to characterize and study the Mn^{2+} doping state and Mn^{2+}-Mn^{2+} interaction in $Mn_xZn_{1-x}Se{\cdot}en_3$. Six well-resolved hyperfine lines, which are attributed to the Mn^{2+} allowed transition imply that the Mn ions were embedded inside $Mn_xZn_{1-x}Se{\cdot}en_3$ lattices and partly replaced Zn. As shown in PL spectrum; the introduction of Mn^{2+} strongly increases the intensity of the PL peak. The internal Mn transition ($^4T_1 \rightarrow {}^6A_1$), which strongly increases the peak intensity depends on the average number of Mn atoms in the nanoparticals. As the Mn-doped concentration increases, the PL peak intensity is enhanced. A series of samples with different Mn-doping concentrations were prepared and studied. Combining the EPR results with PL spectra of the samples prepared, it is believed that under conditions of heating 40 h at 180 °C and controlling Mn^{2+} ion concentration percentage at 2%-3% (x=0.02-0.03) in the compounds, the best doping can be achieved.

Key words: Manganese-doping, Hyperfine structure, Photoluminescence, ZnSe, DMS

I. INTRODUCTION

Nanometer-scale dilute magnetic semiconductor (DMS) crystallites have extensively attracted much attention because of their unique magneto-optical effect and potential applications as optoelectronic materials [1,2]. For instance, manganese-doped II-VI group compound, as a standout magneto-optical material [3-5], shows many useful properties such as giant Faraday rotation effect near the band edge, giant exciton Zeeman splitting, and a magnetic polaron state. These properties result from the s, p-d exchange interaction between band electron/hole and Mn^{2+} $3d^5$ electron [1,6,7]. Meanwhile, the nanometer-scale materials show significant differences compared with bulk material. The phenomenon which is called quantum size effect happens when particle size becomes comparable to or smaller than the exciton Bohr radius (α_B), and is also the result of the confinement of electron-holes to a small volume [8-10]. In Mn^{2+}-doped II-VI group compounds, besides the increasing band gap energy E_g with the deceasing size, the spatial confinement of the electron and hole and the corresponding increase in their overlap with the localized d-electron states provide fast energy transfer of electron-hole pairs to the Mn^{2+} impurity and subsequently lead to large photoluminescent efficiency and much faster radiative recombination of d-electron excitation than in the bulk crystals [11,12].

Based on these properties, some more complicated Mn^{2+}-doped semiconductors such as quantum-dot solid, light-emitting diode (LED) and even photonic crystals have been invented [13-15]. Such materials are promising for the production of optical sensitizers and photocatalysts [16].

Nanometer-scale DMS has been made by many fabrication techniques, such as molecular beam epitaxy (MBE), electron-beam lithography techniques and solvothermal treatment route [5,17-19]. The of preparation route decides the quality of the resulting semiconductor materials and distribution of dopant atoms which influence their optical and magnetic properties. Compared with solvothermal treatment, MBE and electron-beam lithography techniques need special apparatus like an MBE-growth chamber. Therefore, the solvothermal treatment route is widely used in general preparation, such as the prepartion of ethylenediamine-intercalated layered DMS [1,13]. The ethylenediamine -intercalated layered compounds are a novel type of inorganic/organic (I/O) hybrid structure semiconductors. The covalent organic-inorganic hybrid composites own rigidity, stability and superior electronic, magnetic, and optical properties of inorganic materials and processability, flexibility and structure diversity of organic compounds [20-22]. In a word, combining the useful properties of both organic and inorganic components, new materials which have the semiconducting functionality of the inorganic constituent and the lower weight and volume of the organic component, can be made.

*Author to whom correspondence should be addressed. E-mail: jfchen@ustc.edu.cn, Tel.: +86-551-3602807, Fax: +86-551-3602803

TABLE I Preparation route of $Mn_xZn_{1-x}Se$ precursor

Preparation route	Reagents	Reaction temperature	Reaction time
Traditional [1]	$Zn(CH_3COO)_2$, $(1-x)$ mmol	190 °C	168 h
	$Mn(CH_3COO)_2$, x mmol		
	Se, 1 mmol		
	Ethylenediamine, 10 mL		
Current [13]	$ZnSO_4{\cdot}7H_2O$, $(1-x)$ mmol	180 °C	40 h
	$MnSO_4{\cdot}H_2O$, x mmol		
	Se, 1 mmol		
	Ethylenediamine, 12.5 mL		
	$N_2H_4{\cdot}H_2O$, 2.50 mL		

For Mn^{2+}-doped semiconductors, studies have shown that ferromagnetism may be induced when magnetic Mn is doped into nonmagnetic II-VI. Until now, much effort has been focused on these doped materials such as MnZnX and MnCdX (X=S, Se, Te) [3,5,23]. Mn^{2+} acts as a paramagnetic center (I=5/2) which substitutes for the group II cation in the semiconductor lattice [24]. It is well-known that the hyperfine interaction between the electron and nuclear spin of the Mn^{2+} is strongly dependent on the local environment, and that the EPR spectra can be used to determine the location state of the Mn [25]. The six lines of EPR hyperfine structure in Mn^{2+}-doped ZnSe correspond to the allowed hyperfine transitions (m_s=1/2, $m_I \leftrightarrow m_s$=1/2, m_I) (Δm_s=±1, Δm_I=0), where m_I=−5/2, −3/2, −1/2, +1/2, +3/2, +5/2, and m_s and m_I are electron spin and nuclear spin quantum numbers respectively. Sometimes, when it comes to polycrystalline and disordered materials, five forbidden hyperfine lines come into appearance which are due to forbidden transitions (m_s=1/2, $m_I \leftrightarrow m_s$=−1/2, m_I=−1), and (m_s=1/2, m_I=−1$\leftrightarrow m_s$=−1/2, m_I)(Δm_s=±1, Δm_I=±1), where m_I=−3/2, −1/2, +1/2, +3/2, +5/2 [25,26].

In this work, an improved solvothermal route is reported for the preparation of Mn^{2+}-doped ZnSe ethylenediamine-intercalated precursor nanoribbon bundles ($Mn_xZn_{1-x}Se{\cdot}en_3$). Compared with the traditional route, this improved route is time-saving and efficient. Following the application of the new route, apart from XPS, TGA, FESEM which can show the composite and morphology of the precursor, EPR and PL spectra were used to study the Mn^{2+} doping state and Mn^{2+}-Mn^{2+} interaction in $Mn_xZn_{1-x}Se{\cdot}en_3$ nanoribbon bundles. If six well-resolved hyperfine lines appear in EPR spectrum resulting from the isolated Mn^{2+} and strong PL intensity of the sample appear, it is believed that Mn ions in the sample are efficiently embedded inside the crystal lattices and Mn-doping is successful [6,27,28]. In this experiment, a series of samples with different Mn^{2+}-doping concentrations were prepared and studied. In addition, the reaction time and the heating temperature were also investigated for the sake of finding optimal doping experimental conditions. Finally, it was determined that the best doping for the preparation of $Mn_xZn_{1-x}Se{\cdot}en_3$ nanoribbon bundles can obtained under the condition of heating 40 h at 180 °C in an autoclave.

II. EXPERIMENTS

A. Sample preparation

Preparation of $Mn_xZn_{1-x}Se{\cdot}en_\delta$: All reagents were analytical grade, purchased from the Shanghai Chemical Reagent Co. Ltd, and used without further purification. In the current synthesis, anhydrous ethylenediamine (12.5 mL) was added into an aqueous solution of $MnSO_4{\cdot}H_2O$ and $ZnSO_4{\cdot}7H_2O$ (5 mL, the total mass of cations ($[Zn^{2+}]+[Mn^{2+}]$ is constant and equals 1 mmol) and magnetically stirred for 10 min. (Agitation time was tested in early experiments; the results show that 10 min of agitating is enough for the experiment because final ESR spectra of the samples agitated for 10 and 30 min were identical). Following this, the solution was transferred to a 30 mL stainless steel Teflon-lined autoclave, then selenium (79.8 mg, 1 mmol) and hydrazine hydrate (2.50 mL, $N_2H_4{\cdot}H_2O$) were directly put into the autoclave. It was found that the reaction temperature at 170-190 °C was suitable, at temperatures lower than 120 °C the reaction could not be initiated. The autoclave was sealed and maintained at 180 °C for several hours. In order to get optimal synthesis conditions and the best doping results, a series of experiments with different Mn-doping concentrations and reaction times were done. After the autoclave was cooled to room temperature naturally, the pink precipitates were collected and washed with distilled water and absolute ethanol three times separately and finally dried at 60 °C for 2 h.

Table I lists experimental conditions for two routes in preparing $Mn_xZn_{1-x}Se{\cdot}en_3$. Compared with the traditional route of 168 h, the current way is obviously time-saving since 40 h is sufficient for the reaction. More evidence could be obtained by EPR spectra of the samples prepared using the two routes. The EPR spectrum

DOI:10.1088/1674-0068/20/05/607-612

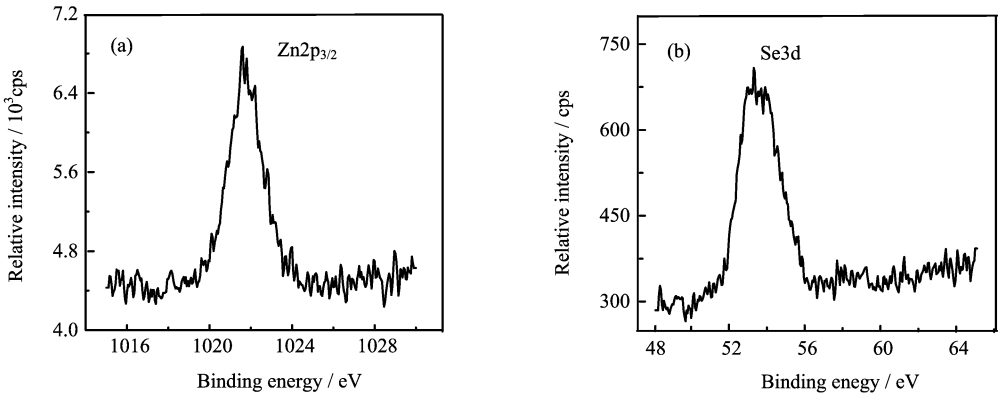

FIG. 1 XPS analysis of the precursor: (a) Zn region, (b) Se region.

of the sample prepared by the traditional route shows a broad symmetrical line and six weak hyperfine lines superimposed upon this main line, which indicates that Mn^{2+}-Mn^{2+} interaction dominates in $Mn_xZn_{1-x}Se{\cdot}en_3$. Some isolated Mn^{2+} exists in this case. In contrast, a sample prepared by the current new route shows six well-resolved hyperfine lines which are attributed to the isolated Mn^{2+}. This means that Mn ions in the sample are efficiently embedded inside the crystal lattices, and good Mn-doping was realized.

B. Characterization

The XPS spectrum was collected by an ESCALab MKII X-ray photoelectron spectrometer with Mg Kα X-ray as the excitation source. To determine the content of ethylenediamine precursor in $Mn_xZn_{1-x}Se{\cdot}en_\delta$, thermo gravimetric analysis (TGA) was done on a TGA-2050 (TA Corp.) thermogravimeter. The general morphology of $Mn_xZn_{1-x}Se{\cdot}en_3$ was observed by field-emission scanning electron microscopy (FESEM; JEOL JSM-6700F SEM), in which the sample was mounted on a copper slice without any dispersion treatment.

C. EPR and PL spectra

Room-temperature Electron paramagnetic resonance (EPR) spectra of $Mn_xZn_{1-x}Se{\cdot}en_3$ were obtained by using a JEOL JES-FA200 EPR spectrometer (X-band, 9063 MHz, 300 K). The microwave power employed was 5 mW (if not specially provided), the sweep width ranged from 286 to 386 mT, the time constant was 0.1 s, and the modulation frequency and modulation width were 100 kHz and 3.5 G, respectively. For the sake of comparison of the doping efficiency and EPR relative intensity, all samples had the same weight. Photoluminescence (PL) spectra were obtained at room temperature using a Perkin-Elmer LS 55 luminescence spectrometer (Perkin-Elmer Co., Ltd., USA) with Rhodamine 101 as the interior standard for luminescence intensity. Measurement conditions were identical in all cases, therefore, the spectra intensities can be compared. Samples with different Mn^{2+}-doping concentrations and heating time (reaction time) were studied and are discussed in the following parts.

III. RESULTS AND DISCUSSION

The evidence for the quality and composition of the product was obtained by X-ray photoelectron spectroscopy (XPS). The very small amount of Mn^{2+} could be neglected. The binding energies obtained in the XPS analysis were corrected for specimen charging by reference the C1s to 284.90 eV. Figure 1 shows the XPS spectra obtained from the Zn and Se regions of the precursor. In Fig.1(a), there is a strong peak at 1022 eV, which is attributed to $Zn2p_{3/2}$. In Fig.1(b), there is a strong peak at about 53 eV, which corresponds to the Se3d. No obvious peaks for other elements or impurities were observed.

According to the results with Eq.(1), it can be calculated from the TGA curve that there was a 56.7% weight loss for this compound, corresponding to loss of ethylenediamine from 100 °C to 700 °C. This yields a value of δ equal to 3 for the precursor, this value being consistent with the result of theoretical calculation for adding ethylenediamine at the beginning.

$$\delta = \frac{(W_{700} - W_{100})/N_{\rm en}}{W_{700}/N_{\rm Mn_xZn_{1-x}Se}} \qquad (1)$$

here, W_{700}: weight of the precursor at 700 °C, W_{100}: weight of the precursor at 100 °C, $N_{\rm en}$: molecular weight of Ethylenediamine, $N_{\rm Mn_xZn_{1-x}Se}$: molecular weight of $Mn_xZn_{1-x}Se$.

Figure 2 clearly indicates that the products are composed of nanoribbon bundles. The observed length of nanoribbon ranges from 10 μm to 20 μm. The ribbon-like morphology of the precursor is closely related to the

DOI:10.1088/1674-0068/20/05/607-612

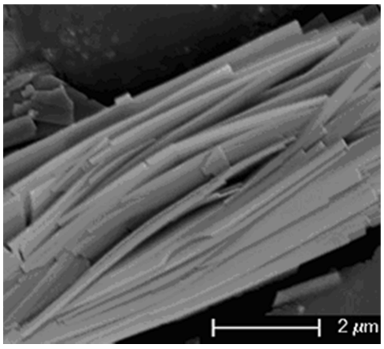

FIG. 2 FESEM images of the as-synthesized Mn^{2+} nanoribbon bundles.

formation process which can be explained as follows:

$$(1-x)Zn^{2+} + 3en \longrightarrow Zn_{(1-x)}en_3{}^{2+} \quad (2)$$
$$xMn^{2+} \longrightarrow Mn_x{}^{2+}$$
$$Se \longrightarrow Se^{2-} \quad (3)$$
$$Mn_xZn_{(1-x)}en_3{}^{2+} + Se^{2-} \longrightarrow Mn_xZn_{1-x}Se \cdot en_3 \quad (4)$$

here, the function of ethylenediamine is not just as one reductive and solvent; it is believed that the prepared $Mn_xZn_{1-x}Se{\cdot}en_3$ is intrinsically related to the template effect of ethylenediamine or so-called assisted effect [13]. Li and coworkers have expatiated the solvent coordination molecular template (SCMT) mechanism which can explain the growth mechanism of CdE (E=S, Se, Te) nanorods in ethylenediamine [29]. Accordingly, in this experiment it was assured ethylenediamine could partly act as a molecular bridge between neighboring $Mn_xZn_{1-x}Se$ chains or layers. Concretely, ethylenediamine which contains more than one N-chelating atom in each molecule possibly combines with Zn^{2+}, Mn^{2+} and Se^{2-} in a line owing to its linear structure. According to reported research [13,17,29], the morphology of the precursor could be directed by changing the ratio of ethylenediamine and water. This conclusion was also proved true in our experiment; the related results are dealt with in process.

Room temperature PL and photoluminescence excitation (PLE) spectrum of undoped $ZnSe{\cdot}en_3$ are shown in Fig.3. From the PLE spectrum (Fig.3(a)), we can see that the maximum exciting wavelength is 303 nm. In order to get a strong signal in the PL spectrum, the exciting wavelength was set as approximately 300 nm, which led to observation of a sharp and stable peak at 588 nm (Fig.3(b)), which usually results from dislocations, stacking faults, and non-stoichiometric defects [13]. $ZnSe{\cdot}en_3$ exhibits efficient emission itself, but compared with Mn-doped $ZnSe{\cdot}en_3$, which can be hundreds times stronger than it, its peak can be neglected. At the same time, the curves of doped samples have the maximum emission peak at 588 nm as well. PL spectra can provide decisive information and determine the electronic-level structure of the Mn^{2+}. In Mn-doped

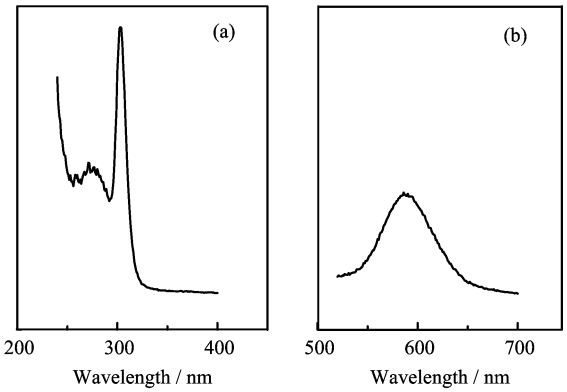

FIG. 3 (a) PLE spectra of undoped $ZnSe{\cdot}en_3$. (b) PL spectra of undoped $ZnSe{\cdot}en_3$ where the spectra have been magnified by 5 times.

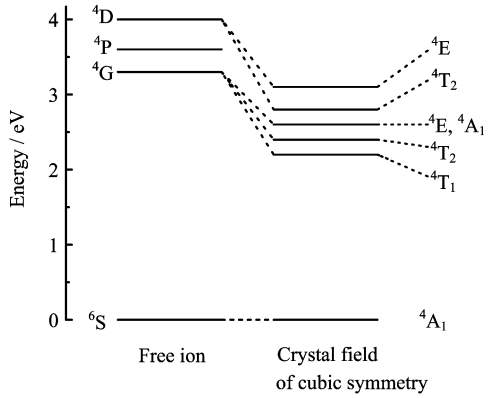

FIG. 4 Energy-level diagram of Mn^{2+} in a free-ion state and in a ZnSe crystal.

ZnSe, Mn^{2+} occupy the sites of Zn^{2+} and have tetrahedral symmetry. Under this symmetry, the first excited state ^4G of Mn^{2+} in a free-ion state is split into $^4T_1$, $^4T_2$, $^4A_1$, and ^4E multiplet states, and $^6A_1(^6S)$ is the ground state. As seen in Fig.4, the great increasing of the peak at 588 nm is attributed to the transition from the $^4T_1(^4G)$ state of Mn^{2+} to the $^6A_1(^6S)$ ground state [5,6].

$Mn_xZn_{1-x}Se{\cdot}en_3$ nanoribbon bundles were prepared with different Mn-doping concentration, and then corresponding EPR spectra were obtained. The EPR spectra of the samples are shown in Fig.5(A). In the doping process for $Mn_xZn_{1-x}Se{\cdot}en_3$, it was found that while $x<0.02$ (curves (c), (d), (e)), six well-resolved hyperfine lines could be observed, which are from the ^{55}Mn nucleus ($I=5/2$) and correspond to the allowed transition ($\Delta m_s=\pm1$, $\Delta m_I=0$), and mean that all the Mn^{2+} ions have a homogeneous environment without Mn^{2+}-Mn^{2+}interaction. With the increase of Mn-doping concentration, the intensity of the six hyperfine lines becomes weak. When $x>0.03$ (curves (a), (b)), an obvious background signal appears. This originates from the electron spin-spin ($m_s=1/2\rightarrow m_s=-1/2$) interac-

DOI:10.1088/1674-0068/20/05/607-612

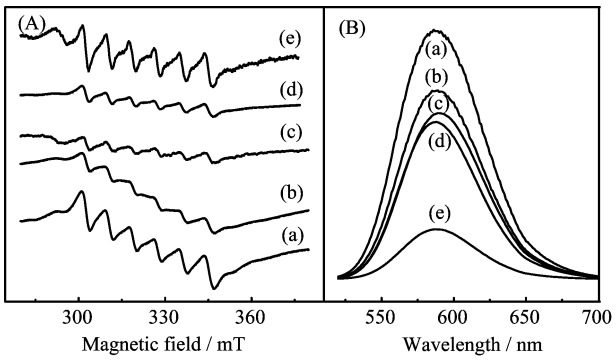

FIG. 5 (A) EPR spectra of $Mn_xZn_{1-x}Se{\cdot}en_3$. (B) PL spectra of $Mn_xZn_{1-x}Se{\cdot}en_3$. (a) $Mn_{0.04}Zn_{0.96}Se{\cdot}en_3$, (b) $Mn_{0.03}Zn_{0.97}Se{\cdot}en_3$, (c) $Mn_{0.02}Zn_{0.98}Se{\cdot}en_3$, (d) $Mn_{0.01}Zn_{0.99}Se{\cdot}en_3$, (e) $Mn_{0.004}Zn_{0.996}Se{\cdot}en_3$.

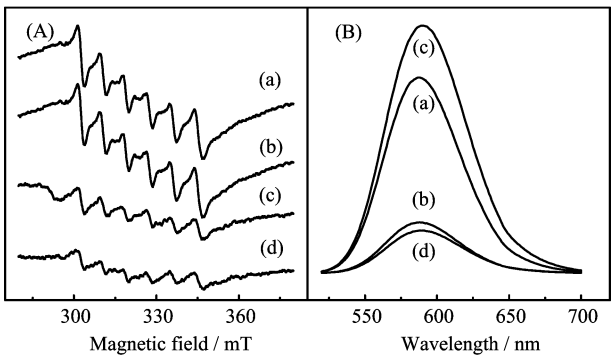

FIG. 6 (A) EPR spectra of $Mn_{0.02}Zn_{0.98}Se{\cdot}en_3$ heated. (B) PL and PLE spectra of $Mn_{0.02}Zn_{0.98}Se{\cdot}en_3$ heated. (a) 80 h, (b) 60 h, (c) 40 h, (d) 10 h.

tions, which indicates that Mn^{2+}-Mn^{2+} interaction has been present, but the isolated Mn^{2+} still dominates the case. In a much higher Mn^{2+} concentration fraction (x>0.06, unshown here), the spectrum would appear as a standard broad EPR spectrum, indicating Mn^{2+}-Mn^{2+} interaction dominates the environment in $Mn_xZn_{1-x}Se{\cdot}en_3$; that is the case we have to avoid [26]. In the experiment, another thing was noticed: the precursor samples could not be milled. The 6 hyperfine lines of EPR spectrum would disappear after milling, which can be explained by distortion of the crystal lattice. To identify Mn^{2+} location in the sample, the value of hyperfine splitting constant, α, is quoted in cm^{-1}. The conversion can be made using:

$$\alpha = \alpha(\text{in Gauss}) \times g \times \beta \qquad (5)$$

where β=4.67×$10^{-5}$$cm^{-1}G^{-1}$. We can extract a hyperfine splitting of 67.6×10^{-4} cm^{-1} using this equation. This value agrees well with that obtained for Mn at cubic sites in bulk ZnSe (61.7×10^{-4} cm^{-1}) [24], so it is thought that most of the Mn ions substitute for Zn ions in the compounds.

The internal Mn transition ($^4T_1 \rightarrow {}^6A_1$) strongly increases the peak intensity which depends on the average number of Mn atoms in the nanoparticles [6,9,26-34]. Shown in Fig.5(B), the peak intensity of PL spectrum enhances as the Mn-doping concentration increases [32]. But increasing concentration will lead eventually to fluorescence quench. As is understood, an isolated Mn^{2+} is a strong luminescence center, and the enhancement of Mn^{2+}-Mn^{2+} interaction due to their close proximity is responsible for the Mn^{2+} luminescence quench [25]. According to the PL and EPR spectra of the samples, we might surely conclude that when x<0.04, the isolated Mn^{2+} can more readily exist in the lattices of $Mn_xZn_{1-x}Se{\cdot}en_3$ nanoribbon bundles.

Heating time is another important factor which affects the Mn-doping state. Too short or too long time heating is not suitable for the formation of DMS while keeping the heating temperature the same, so the process requires a suitable heating time. A number of experiments were performed in the present study. Figure 6 (A) and (B) are the EPR and the PL spectra of the as-prepared samples respectively, with samples heated at 180 °C for different time durations. It can be seen that if the sample was heated too short time, the intensity of the hyperfine line was too weak (Fig.6(A), curve (d)); while if the heating time was too long, obvious background came into appearance (Fig.6(A) curve (a), (b)). In curve (a), we can also see that there exist several weak lines between the six intense lines, which can be assigned to double spin transition (Δm_s=±1, Δm_I=±1) where both m_s and m_I change simultaneously [26]. From the PL spectrum shown in Fig.6(B), it was found that the strongest peak came from heating the sample for 40 h when all samples were made in the same conditions except for heating time. The results could possibly be explained by Mn^{2+}-Mn^{2+} exchange interaction in the samples. When the sample was heated too long, Mn could be deeply embedded in the $Mn_xZn_{1-x}Se{\cdot}en_3$ lattice, and then the Mn^{2+}-Mn^{2+} exchange interaction could be strengthened and lead to luminescence quench. Based on this data, the suitable heating time selected for the preparation was about 40 h in the doping process.

IV. CONCLUSION

In this work, Mn^{2+}-doped ZnSe ethylenediamine-intercalated precursor nanoribbon bundles were successfully synthesized through an improved solvothermal route in an autoclave at 180 °C for 40 h. FESEM images showed the length of $Mn_xZn_{1-x}Se{\cdot}en_3$ nanoribbon bundles ranged from 10 μm to 20 μm. In addition, the optimal conditions such as dopant concentration, reaction temperature and heating time for Mn doping was determined through combining the analysis of the EPR and PL spectra for the objective products, The results show that under condition of heating 40 h at

DOI:10.1088/1674-0068/20/05/607-612

180 °C and 2%-3% Mn^{2+} doping concentration percentage (x=0.02-0.03) the synthesis of $Mn_xZn_{1-x}Se{\cdot}en_3$ nanoribbon bundles leads to the best doping. Where there is limited Mn-doping concentration, the introduction of Mn strongly increases the intensity of the PL emission peak. In contrast, a large component of Mn^{2+} and long time heating leads to the increase of Mn^{2+}-Mn^{2+} interaction that quenches the luminescence.

Compared with traditional route, the improved solvothermal route for manganese-doping is very valuable as it has other main advantages: (i) It is low-cost and has easy operation. (ii) The modality of the nanoparticles can be adjusted though changing the ratio of ethylenediamine /or other amine and water. (iii) The strategy could be extensively used in preparing other nanoscaled doping materials. (iv) The precursors prepared in the route have good stability. This method will contribute to semiconductor production and has great potential in future research and industrial applications.

V. ACKNOWLEDGMENTS

This work was supported by the National Natural Science Foundation of China (No.20621061 and No.20473082), and the Anhui Provincial Natural Science Foundation (070414195).

[1] J. Lu, S. Wei, W. C. Yu, and Y. T. Qian, Chem. Mater. **17**, 1698 (2005).
[2] N. Takahashi, K. Takabayashi, and E. Shirado, J. Crys. Grow. **214/215**, 183 (2000).
[3] Y. H. Li, B. G. Wang, and S. L. Fu, Chem. Rese. Appl. **12**, 5 (2000).
[4] C. M. Jin, K. Dou, and S. G. Hou, Chin. J. Lumin. **16**, 177 (1995).
[5] Y. H. Zhang, L. Li, and X. F. Shao, J. Func. Mater. **4**, 405 (2001).
[6] M. Tanaka, J. Lumi. **100**, 163 (2002).
[7] X. Chen, X. Z. Wang, and J. Z. Liu, Chin. J. Semi. **17**, 573 (1996).
[8] I. Yu, T. Isobe, and M. Senna, J. Phys. Chem. Solids. **57**, 373 (1996)
[9] K. Sooklal, B. S. Cullum, S. M. Angel, and C. J. Murphy, J. Phys. Chem. **100**, 4551 (1996).
[10] Y. M. Chen, W. D. Xiang, and L. D. Sun, J. Lumin. **16**, 362 (1995).
[11] R. N. Bhargava, D. Gallagher, X. Hong, and A. Nurmikko, Phys. Rev. Lett. **72**, 416 (1994).
[12] B. B. Stojic, D. Milivojevic, and V. Vodnik, J. Phys.: Condens. Matter. **16**, 4625 (2004).
[13] S. L. Xiong, J. M. Shen, Q. Xie, and Y. T. Qian, Adv. Funct. Mater. **15**, 1787 (2005).
[14] J. M. Huang, Y. Yang, and S. H. Xue, Appl. Phys. Lett. **70**, 2335 (1997).
[15] B. O. Dabbousi and M. G. Bawendi, Appl. Phys. Lett. **66**, 1316 (1995).
[16] D. Denzler, M. Olschewski, and K. Sattler, J. Appl. Phys. **84**, 2841 (1998).
[17] X. Wang, J. Zhuang, Q. Peng, and Y. D. Li, Nature, lett. **437**, 121 (2005).
[18] Z. J. Wang, H. M. Zhang, and L. G. Zhang, Chin. J. Lumin. **23**, 364 (2002).
[19] L. Q. Yue, H. F. Zhou, and Y. Y. Hao, Chin. J. Lumin. **26**, 189 (2005).
[20] X. Y. Huang and J. Li, J. Am. Chem. Soc. **122**, 8789(2000).
[21] P. D. Yang, D. Y. Zhao, D. I. Margolese, and B. F. Chmelka, Nature **396**, 152 (1998).
[22] M. O'Keeffe, M. Eddaoudi, and O. M. Yaghi, J. Solid. State. Chem. **152**, 3(2000).
[23] Harry R. Heulings IV, X. Y. Huang, and J. Li, Nano Lett. **1**, 521 (2001).
[24] D. J. Norris, N. Yao, and T. A. kennedy, Nano. Lett. **1**, 3 (2001).
[25] S. C. Erwin, L. J. Zu, and M. I. Haftel, Natu. Lett. **436**, 912005.
[26] I. Yu and M. Senna, Appl. Phys. Lett. **66**, 424 (1995).
[27] M. Jain and J. L. Robins, *in Diluted Magnetic Semiconductors*, M. Jain, Ed., Singapore: World Scientific, (1991).
[28] M. A. Chamarro, V. Voliotis, and R. Grousson, J. Cryst. Growth **159**, 853(1996).
[29] Z. X. deng, C. H. Wang, X. M. Sun, and Y. D. Li, Inorg. Chem. **41**, 869 (2002).
[30] H. Y. Lu, S. Y. Chun, and S. S. Tan, Jpn. J. Appl. Phys. **44**, 5282 (2005)
[31] W. Chen, F. H. Su, and G. H. Li, J. Appl. Phys. **92**, 1950 (2002).
[32] L. Chen, J. H. Zhang, and Y. S. Luo, Appl. Phys. Lett. **84**, 112 (2004).
[33] H. Yang, Z. C. Wang, and L. W. Wang, Chin. J. Mater. Rese. **10**, 541 (1996).
[34] S. L. Ren, J. H. Zhang, and S. Z. Lv, Chin. J. Lumin. **23**, 451 (2002).

DOI:10.1088/1674-0068/20/05/607-612